



Effects of mooring line hydrodynamic coefficients and wave parameters on the floating production storage and offloading motions

Zhiyang Zhang^a, Haitao Wu^{b,*}, Weixing Liu^a

^a*School of Ocean Engineering, Jiangsu Ocean University, Lianyungang 222005, China*

^b*School of Naval Architecture, Ocean & Civil Engineering, Shanghai Jiao Tong University, Shanghai 200240, China, email: wuhaitao19960912@163.com*

Received 17 August 2021; Accepted 23 September 2021

ABSTRACT

As the main facility for offshore oil and gas development, floating production storage and offloading (FPSO) has received great attention from researchers and engineers. This paper relies on a time-domain analysis code to investigate the effects of mooring line hydrodynamic coefficients and wave parameters on the FPSO motions. In order to verify the reliability of this code, the hydrodynamic software AQWA is used for comparison. Under the irregular wave, it can be found that the results calculated by these two numerical tools are in good agreement. After that, two cases concerning the hydrodynamic coefficients and wave parameters are created. Finally, the sensitivity of the FPSO motions to mooring line hydrodynamic coefficients and wave parameters are discussed. The results show that the mooring line hydrodynamic coefficients and wave parameters have a significant influence on the FPSO dynamic behavior. However, among the results, it can be found that the wave-frequency motions are not affected by the hydrodynamic coefficients of the mooring line due to the turret-moored configuration. In general, they are of great help for the initial design of the FPSO system.

Keywords: Floating production storage and offloading motions; Mooring line hydrodynamic coefficients; Wave parameters; Standard deviation; Response spectrum

1. Introduction

Floating production storage and offloading (FPSO) is a large offshore oil production platform that can carry out oil and gas separation, crude oil storage and transportation. FPSO has advantages over other types of offshore platforms in the construction period, wind resistance, fuel consumption, storage capacity. FPSO has become the main production facility for offshore oil field development. Since FPSO works in areas with harsh sea conditions for a long time, this poses a serious challenge to the working ability of FPSO. The large amplitude of vertical motions of FPSO poses a threat to the safety of people on the board, while the horizontal motions with a large natural period have a significant influence on the mooring system and

risers. In addition, in areas with variable sea conditions, frequent strenuous motions severely shorten the fatigue life of mooring systems and risers. Therefore, the mooring system and risers should be selected according to the environmental conditions of the working sea area to predict the dynamic behavior of FPSO.

In the past decades, scholars have studied the motions of floating platforms from uncoupled analysis to coupled analysis. Under the combined loads of wind, wave, and current, Wichers [1] started the study on the dynamic response of FPSO by performing uncoupled analysis. Jiang and Schellin [2] developed a time-domain coupled code to study the low-frequency and wave-frequency motions of FPSO and explained the phenomenon of slow-drift motions in the horizontal plane. Heurtier et al. [3] used uncoupled analysis and coupled analysis to conduct a comparative study

* Corresponding author.

on FPSO motion, and concluded that the uncoupled analysis is sufficient for the mooring system initial design. In shallow water, the indicated accurate result can be obtained without including the damping of the mooring system [4]. In this case, the uncoupled analysis method shows advantages in saving computing resources. However, when the water depth increases, the mooring lines significantly contribute to the damping of the floating system. If the mooring-induced damping is still not considered, the motions of the floating structure and the mooring line tension can be greatly affected. In addition, as the water depth increases, the added mass of the mooring line also increases, which cannot be ignored either. Through the comparative study of non-coupling analysis and coupling analysis, it was found that there is a big discrepancy in low-frequency surge motion and mooring line tension [5–8]. Ormberg and Larsen [9] and Tahar et al. [10] found that the uncoupled analysis method overestimates the low-frequency responses and mooring line tension. Therefore, in order to obtain an accurate dynamic response in deep water, a coupled dynamic analysis is often used. This method takes into account the interaction between platform motion and mooring line dynamics and can reflect the real situation to a certain extent. A coupled analysis method to study the effects of incident wind/wave directions on the dynamic behavior of a wind turbine system [11].

A studied the influence of the hydrodynamic coefficient of the mooring line on the FPSO motions through a fully-coupled dynamic analysis method [12]. The results showed that as the hydrodynamic coefficient increases, the low-frequency motion and mooring line tension decrease. Mohammed et al. [13] that the hydrodynamic damping of the mooring system is important for the coupled model. With or without drag and inertial force on the mooring line, the dynamic behavior of the Spar platform changes significantly. In the process of investigating the influence of wave parameters on the motion of a semi-submersible platform, a study concluded that the wave height has a significant influence on the surge motion, while the wave period plays a vital role in the heave motion [14]. Some believed that the mooring damping cannot be ignored in the process of studying the FPSO motion [15]. The horizontal motions of the FPSO decrease with the increase in the wave height, while the vertical motions increase linearly with the wave height [16–19]. When analyzing the contribution of the low-frequency component to the fatigue damage of the mooring line, Du et al. [20] revealed that an increase in the wave height or a decrease in the wave period would aggravate the fatigue damage.

In this paper, a coupled time-domain analysis code is adopted to study the effects of the mooring line hydrodynamic coefficients and wave parameters on the FPSO motion. The analysis process is helpful to understand the FPSO performance changes with different mooring line hydrodynamic coefficients and wave parameters from the mechanism level. The relevant results can be used for the initial design of the FPSO system.

2. Theoretical background

In time-domain simulations, FPSO is regarded as a rigid body subject to constraints and external forces. Regardless

of the effects of wind and current, the external forces experienced by the FPSO include first-order and second-order wave excitation forces, as well as mooring forces. Therefore, its motion equation in the time domain can be expressed as:

$$[M + A_\infty] \ddot{x}(t) + \int_0^t K(\tau) \dot{x}(t - \tau) d\tau + Cx(t) = F_W^{(1)} + F_W^{(2)} + F_M \quad (1)$$

where $x(t)$, $\dot{x}(t)$ and $\ddot{x}(t)$ refer to the displacement, velocity and acceleration of the platform respectively, M is a mass matrix, A_∞ is the added mass matrix at infinite frequency, C is the hydrostatic stiffness matrix, $F_W^{(1)}$ and $F_W^{(2)}$ are the first-order and second-order wave excitation forces, and F_M is the mooring force. The convolution term in the equation represents the fluid memory effects. $K(t)$ is the retardation function, which can be gained from radiation damping $R(\omega)$:

$$K(t) = \frac{2}{\pi} \int_0^\infty R(\omega) \cos(\omega t) d\omega \quad (2)$$

An irregular wave is obtained by linear superposition of multiple regular waves with random phases, which can be expressed as:

$$\zeta(x, t) = \sum_{i=1}^N A_i \cos(k_i x - \omega_i t + \varepsilon_i) \quad (3)$$

where ε_i is the initial phase angle, evenly distributed in the interval $[0, 2\pi]$. In addition, ω_i and k_i satisfy the dispersion relation:

$$\omega_i^2 = gk_i \tanh(k_i h) \quad (4)$$

When the wave spectrum is determined, the i -th wave amplitude can be written as:

$$A_i = \sqrt{2S(\omega_i) \Delta\omega_i} \quad (5)$$

In the time domain, the first-order wave excitation can be expressed as [21]:

$$F_W^{(1)}(t) = \text{Re} \sum_{i=1}^N A_i Q(\omega_i) e^{i\omega_i t} \quad (6)$$

where $Q(\omega_i)$ is the first-order wave excitation transfer function.

The second-order difference-frequency wave excitation force can be obtained by the double Fourier-transform [22]:

$$F_W^{(2)}(t) = \text{Re} \sum_{i=1}^N \sum_{j=1}^N A_i A_j^* Q - (\omega_i, \omega_j) e^{i(\omega_i - \omega_j)t} \quad (7)$$

where $(*)$ refers to the complex conjugate, and $Q - (\omega_i, \omega_j)$ is the low-frequency wave excitation quadratic transfer functions (QTFs).

In order to save computational resources, the Newman approximation method is used to solve the QTF matrix [23]. The off-diagonal values of the matrix can be approximated by the diagonal values:

$$Q-(\omega_i, \omega_j) = \frac{1}{2} [Q-(\omega_i, \omega_i) + Q-(\omega_j, \omega_j)] \quad (8)$$

In this code, it is assumed that no torque and external moment is applied on the mooring line. Based on the lumped-mass method, the mooring line is modeled as N evenly-sized segments connecting $N+1$ nodes. The cable segment between nodes i and $i+1$ is indexed with $i+1/2$. The motion equation of node i is derived as follows:

$$(m_i + a_i) \ddot{r}_i = T_{i+1/2} - T_{i-1/2} + C_{i+1/2} - C_{i-1/2} + W_i + B_i + D_{pi} + D_{qi} \quad (9)$$

where m_i and a_i are the node i mass matrix and added mass matrix, respectively. n refers to the displacement vector.

In addition, $T_{i+1/2}$ and $T_{i-1/2}$ are the tension of segments $i+1/2$ and $i-1/2$ respectively. $C_{i+1/2}$ and $C_{i-1/2}$ are the internal damping force. W_i is the weight force, and B_i is the contact force. D_{pi} and D_{qi} are the transverse and tangential drag forces. The detailed formulation of the mooring line model can be found by the study of Hall and Goupee [24].

The hydrodynamic coefficients such as the added mass, the radiation damping, and the first- and second-order wave excitation force transfer functions can be obtained by the frequency-domain simulation. Then, they are transformed into the retardation function and external force in the time domain simulation through inverse Fourier transform (IFT) and convolution technique for solving Eq. (1). As for the specific algorithm to solve Eq. (1), the Newmark method is adopted in this code. α and β are two weighting constants that can be adjusted in Eqs. (10) and (11). The correlations of displacement, velocity and acceleration vectors of the platform can be expressed as follows:

$$\dot{x}(t + \Delta t) = \dot{x}(t) + [(1 - \alpha)\ddot{x}(t) + \alpha\ddot{x}(t + \Delta t)]\Delta t \quad (10)$$

$$x(t + \Delta t) = x(t) + \dot{x}(t)\Delta t + \left[\left(\frac{1}{2} - \beta \right) \ddot{x}(t) + \beta\ddot{x}(t + \Delta t) \right] \Delta t^2 \quad (11)$$

3. FPSO and mooring system

The FPSO operates at a water depth of 120 m and adopts a 3×3 mooring arrangement. Each group of mooring lines are separated by 120° , and the angle between adjacent mooring lines is 5° . Fig. 1 shows a sketch of the FPSO system. From the anchor point to the fair lead, each mooring line is composed of a chain-wire-chain-wire. The suspending chain is equipped with three additional chains with the same parameters to increase the restoring stiffness of the mooring system. The specific parameters of the FPSO and mooring line are shown in Tables 1 and 2, respectively.

4. Validation of the coupled time-domain analysis code

The verification in the time domain is performed by comparing this code with the commercial software AQWA. In this code, the added mass, radiation damping, and first- and second-order wave excitation transfer functions used to calculate the hydrodynamic load of the FPSO are obtained through the frequency module of AQWA. Since there are

Table 1

The parameters of floating production storage and offloading

Term	Value
Length between perpendiculars (m)	267
Breadth (m)	50
Depth (m)	25.1
Draft (m)	16.5
Longitudinal center of gravity (forward) (m)	117.65
Vertical center of gravity (from the keel) (m)	135.65
Radius of inertia around x-axis (m)	14.3
Radius of inertia around y-axis (m)	17.0
Radius of inertia around z-axis (m)	68.4
Displacement (t)	170,431

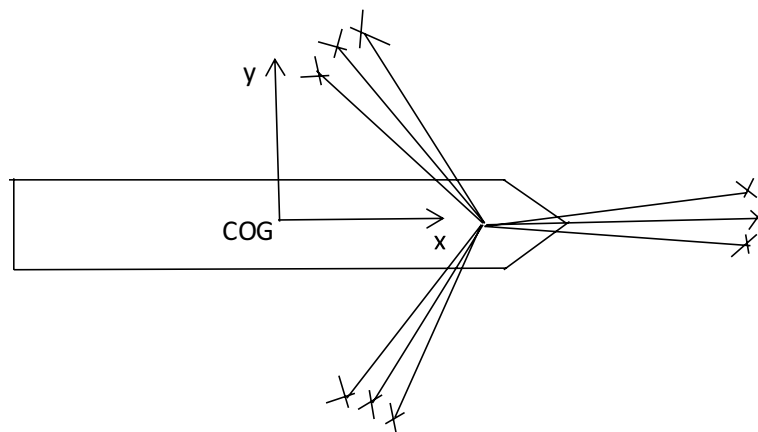


Fig. 1. The sketch of the floating production storage and offloading system.

some discrepancies in the mooring line model and numerical integration method between this code and AQWA, the results of the two numerical tools may not agree well with each other. Therefore, it is necessary to conduct the time-domain verification under the irregular wave. If the calculation results of these two numerical tools are similar, this code can be considered reliable. The significant wave height and spectral peak period of the irregular wave are 9 m and 15 s, respectively. As shown in Fig. 2, the results obtained from this code agree well with those of AQWA. Therefore, the time-domain coupled analysis code can be used for subsequent research.

5. Numerical simulations and research cases

In the time domain, the JONSWAP spectrum is used to simulate irregular waves, which can be expressed as:

$$S(\omega) = \alpha H_s^2 \frac{\omega^{-5}}{\omega_p^{-4}} \exp \left[-\frac{5}{4} \left(\frac{\omega}{\omega_p} \right)^{-4} \right] \gamma \exp \left[\frac{1}{2} \left(\frac{\omega - \omega_p}{\sigma \omega_p} \right)^2 \right] \quad (12)$$

where α is the spectral parameter, H_s is the significant wave height, ω_p is the spectral peak frequency, and γ is the peak-edness parameter. The spectral width parameter σ is 0.07 when $\omega > \omega_p$, and 0.09 when $\omega < \omega_p$.

Under the 3 h short-term forecast, the motion response of the floating structure obeys the Rayleigh distribution,

and the Rayleigh distribution has only one variance. For a given wave spectrum, the wave-frequency motion response spectrum of a floating structure at zero speed can be expressed as:

$$S_R(\omega) = \text{RAO}^2 S(\omega) \quad (13)$$

where RAO is the response amplitude operator. Then, the square of standard deviations (STD) of the wave-frequency motion response is:

$$\text{STD}^2 = \int_0^\infty S_R(\omega) d\omega = \int_0^\infty \text{RAO}^2 S(\omega) d\omega \quad (14)$$

Table 2
The parameters of mooring system

Term	Mooring system			
	Chain	Wire	Chain	Wire
Segment				
Length (m)	51	501	101	251
Diameter (mm)	142	134	142	134
Weight per unit length in water (kN/m)	3.473	0.733	3.473 × 3	0.733
Axial stiffness (kN)	1.19E6	1.78E6	1.19E6	1.78E6
Minimum breaking strength (kN)	17,400	17,800	17,400	17,800

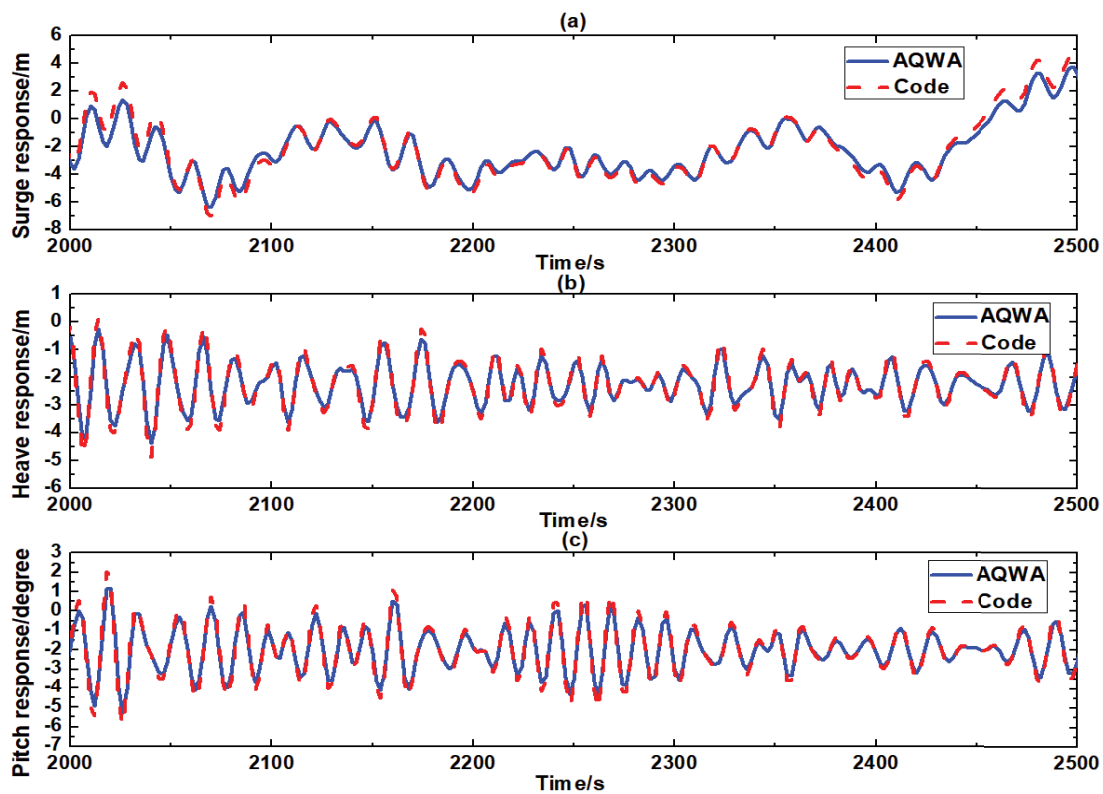


Fig. 2. The floating production storage and offloading motions of this code and AQWA.

The low-frequency wave force response spectrum can be expressed [25]:

$$S_{F,\alpha}^{2-}(\Delta\omega) = 8 \int_0^\infty S(\omega)S(\omega + \Delta\omega) |T_\alpha(\omega; \omega + \Delta\omega)|^2 d\omega \quad (15)$$

where $T_\alpha(\omega; \omega + \Delta\omega)$ is the quadratic transfer function (QTF) of low-frequency wave force.

Once the low-frequency wave force spectrum of a particular sea state is calculated, the second-order low-frequency response spectrum $S_\alpha(\omega)$ of the degree of freedom α is determined by the product of the squared unitary force transfer function $H_{\alpha k}(\omega)$ and the spectrum $S_{F,\alpha}^{2-}(\omega)$ defined in Eq. (15) [26]:

$$S_\alpha^{2-}(\omega) = |H_{\alpha k}(\omega)|^2 S_{F,\alpha}^{2-}(\omega) \quad (16)$$

where,

$$H_{\alpha k}(\omega) = \frac{1}{-\omega^2 [M_{\alpha k} + A_{\alpha k}(\omega)] + i\omega [B_{\alpha k}(\omega) + B'_{\alpha k}] + (C_{\alpha k} + C'_{\alpha k})} \quad (17)$$

This transfer function contains all the dynamic characteristics of the floating system. A , B and C are the added mass, radiation damping and hydrostatic restoration matrixes respectively, and α and k vary from 1 to 6. $B'_{\alpha k}$ is the viscous damping, and $C'_{\alpha k}$ is the external stiffness brought by the mooring lines. Thus, the square of STD of the low-frequency motion response is:

$$STD^2 = \int_0^\infty S_\alpha^{2-}(\omega) d\omega = \int_0^\infty |H_{\alpha k}(\omega)|^2 S_{F,\alpha}^{2-}(\omega) d\omega \quad (18)$$

Two research cases are set to study the effects of mooring line hydrodynamic coefficients and wave parameters on FPSO motion. For the chain and wire, C_{a1} and C_{a2} are the added mass coefficients, C_{dtr1} and C_{dtr2} are the transverse drag coefficients, and C_{dta1} and C_{dta2} are the tangential coefficients. Specific values with respect to the cases are presented in Table 3.

6. Results and discussion

Firstly, the frequency module of AQWA is used to obtain the hydrodynamic coefficients for the time-domain simulation of the coupled analysis code. Then, the corresponding hydrodynamic coefficients are input into the code to perform the coupling analysis under the above two cases. The time-domain simulation under each wave condition requires a 3-h short-term forecast. Finally, a digital filter is compiled to decouple the time history into low-frequency (<0.2 rad/s) and wave-frequency (>0.2 rad/s) components, and then the STD of these two components are gained. In addition, the time histories are converted into the corresponding motion response spectra through fast Fourier transform (FFT). A technical route for the study in this paper is presented in Fig. 3.

6.1. STDs of the FPSO motions under cases 1 and 2

Fig. 4 shows the STDs of the surge, heave and pitch motions under cases 1a and 2a. It can be found that there is a low-frequency component in the surge motion, while the heave and pitch motions do not. This is because the degrees of freedom of heave and pitch are wave-frequency motions and have no low-frequency responses. The wave-frequency STD has a linear relationship with H_s . The low-frequency STD and the total frequency STD of the surge motion have a quadratic relationship with H_s . However, due to the addition

Table 3
Research cases

Case 1	$C_{a1} = C_{a2} = 1, C_{dtr1} = 2.4, C_{dtr2} = 1.2, C_{dta1} = C_{dta2} = 0.2$	Case 2	$C_{a1} = C_{a2} = 1.4, C_{dtr1} = 2.8, C_{dtr2} = 1.6, C_{dta1} = C_{dta2} = 0.4$
	H_s/m	H_s/m	T_p/s
Case 1a	9, 10, 11, 12, 13	Case 2a	9, 10, 11, 12, 13
Case 1b	11	Case 2b	11
	T_p/s		T_p/s
	15		15
	13, 14, 15, 16, 17		13, 14, 15, 16, 17

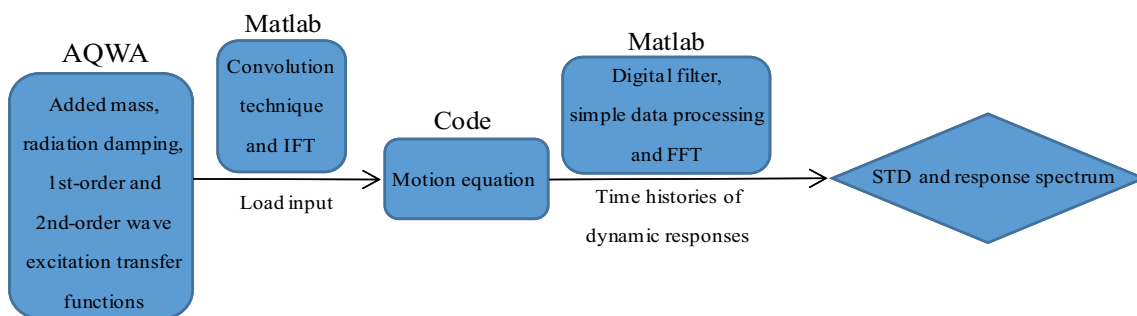


Fig. 3. The technical route for the study.

of the wave-frequency component, the curvature of the total-frequency (TF) STD curve is smaller than that of the low-frequency STD. Under different mooring line hydrodynamic coefficients, the wave-frequency STD does not change. However, the low-frequency and total-frequency STDs of the surge response decrease as the hydrodynamic coefficients increase. Based on the above analysis, it can be concluded that under the wave conditions with different H_s , the sensitivity of the FPSO surge motion to the large mooring line hydrodynamic coefficients decreases, while the sensitivity of the heave and pitch motions remains unchanged. In addition, It can be found that the variation trend of the pitch motion STD is more obvious than that of the heave motion STD. This is because the natural frequency of the

pitch motion is close to the spectral peak period. The degree of freedom of surge is a slow drift motion, with a small natural frequency. Although the low-frequency wave force is much smaller than the wave-frequency wave force in magnitude, it may resonate with the slow drift motion, causing a significant displacement of the floating structure. This phenomenon will over-tension the mooring lines and risers, which will threaten the safety of the floating system. It can be observed in Fig. 4 that as H_s increases, the increase in low-frequency STD becomes more obvious. This means that under severe sea conditions, the magnitude of the low-frequency wave force increases significantly.

Fig. 5 shows the STDs of the surge, heave and pitch motions under cases 1b and 2b. From Fig. 5a, it can be

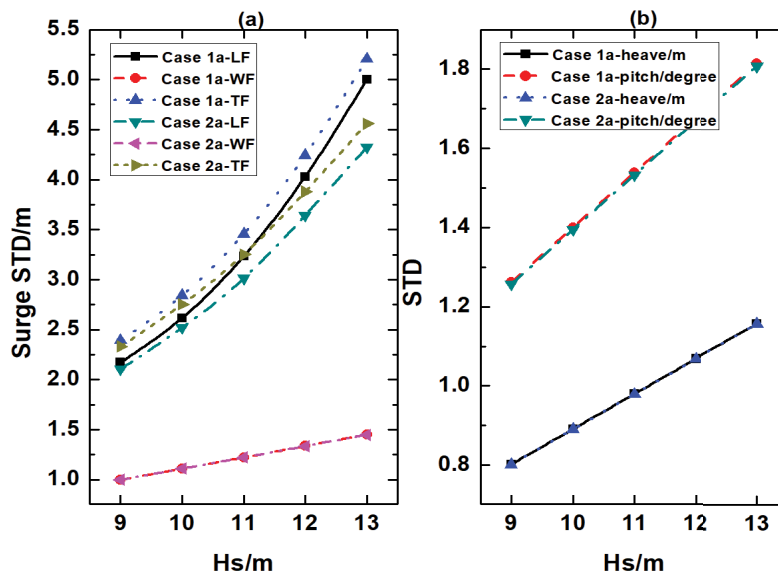


Fig. 4. Standard deviations of the floating production storage and offloading motions under cases 1a and 2a.

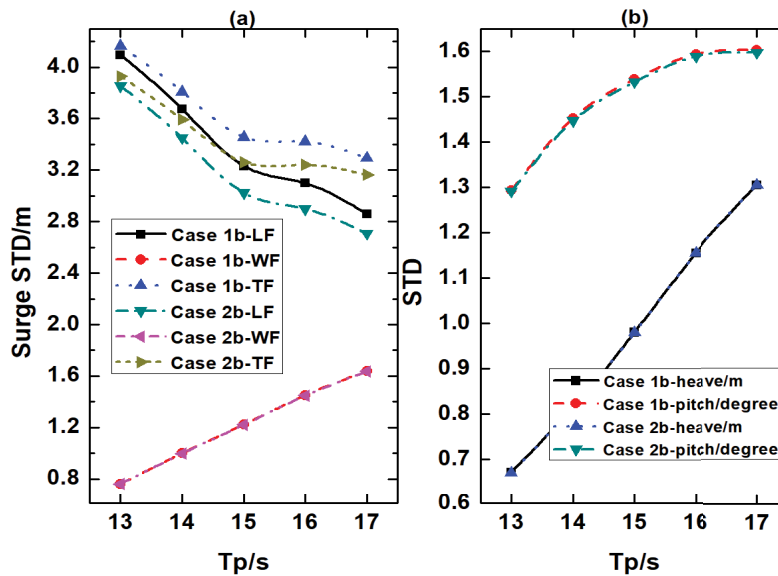


Fig. 5. Standard deviations of the floating production storage and offloading motions under cases 1b and 2b.

found that as T_p increases, the surge low-frequency STD decreases, and the wave-frequency STD increases roughly linearly. In addition, it can be inferred that as the hydrodynamic coefficients of the mooring line increase, the low-frequency STD decreases. Therefore, the hydrodynamic coefficients of the mooring line increase, the sensitivity of the FPSO motions to the wave conditions with different T_p decreases. However, the wave-frequency STD does not change. It can be observed from Fig. 5b that as T_p increases, the heave STD increases roughly linearly. The pitch STD also increases but the increasing trend weakens. Similar to the surge wave-frequency STD, the heave and pitch STDs do not change with the increase in the mooring line hydrodynamic coefficients. So the sensitivity of the heave and pitch motions remains unchanged.

6.2. Effects of mooring line coefficients on the FPSO motions

From section 6.1, it can be found that under large mooring line hydrodynamic coefficients, the STD of the low-frequency response decreases and the STD of the wave-frequency response remains constant. In order to study the effects of different mooring line hydrodynamic coefficients on the FPSO dynamic behavior, a typical sea state ($H_s = 11$ m, $T_p = 15$ s) is specially selected.

From Fig. 6a it can be found that as the hydrodynamic coefficients increase, the peak of the low-frequency component of the surge response spectrum decreases, but the corresponding frequency remains unchanged. The increase in the hydrodynamic coefficients causes H_{ak} to decrease in Eq. (17). Therefore, according to Eq. (16), it can be inferred as the hydrodynamic coefficients increase, the area of the low-frequency surge response spectrum decreases. As for why H_{ak} is reduced, this should be analyzed from the contribution of the added mass coefficient C_a and the drag coefficient C_d to Eq. (17). The added mass coefficient increases, causing H_{ak} to increase. The drag coefficient increases, leading to a decrease in H_{ak} . But overall, the drag coefficient contributes more to Eq. (17), which in turn makes H_{ak} decrease. The coefficient of the added mass term is ω^2 , and that of the damping term is ω . At the low-frequency range, the effects of increased damping on H_{ak} is more obvious. In addition, it can be found from Fig. 6 that the wave-frequency component of the surge response spectra, the heave and pitch response spectra do not change with the increase in the hydrodynamic coefficients. According to Eq. (13), it can be inferred that their RAOs remain unchanged. Because this FPSO adopts a single-point-mooring (SPM) configuration, the increase in the hydrodynamic coefficients of the mooring line cannot change the characteristics of wave-frequency motions.

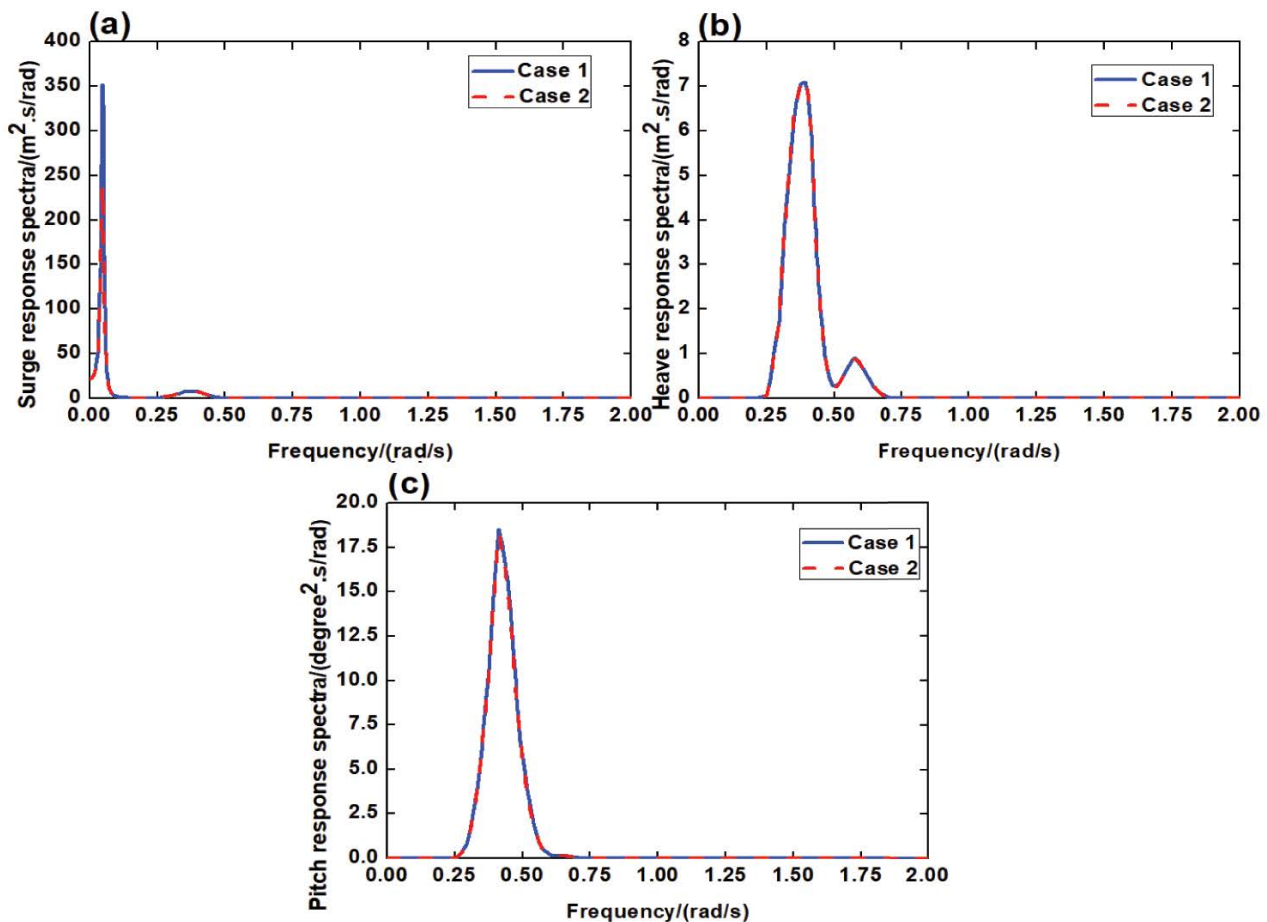


Fig. 6. The floating production storage and offloading motions under cases 1 and 2.

6.3. Effects of wave parameters on the FPSO motions

From section 6.1, it can be found that the wave parameters have a significant influence on the FPSO motions. In order to study the effects of wave parameters on the FPSO motions, case 1a concerning the significant wave height and case 1b concerning the spectral peak period are selected. In addition, the RAOs of the FPSO motions are obtained from the frequency-domain simulations in AQWA.

Fig. 7a shows the wave spectra under case 1a. It can be found that with the increase in H_s , the spectral peak becomes larger, the peak frequency remains unchanged, and the spectral shape becomes wider. Fig. 7b–d show the surge, heave and pitch response spectra. In Fig. 7b, as H_s increases, the peak of the low-frequency component becomes larger, and the corresponding frequency shifts to the right. According to Eq. (15) and Fig. 7a, the wave spectral term $S(\omega)S(\omega + \Delta\omega)$ increases as H_s increases. With an increase in H_s , the shape of the wave spectrum becomes wider, so the difference-frequency component $\Delta\omega$ becomes larger. The increase in $\Delta\omega$ causes the maximum value of $S(\omega)S(\omega + \Delta\omega)$ to shift to the right. From Fig. 7b, it can be observed that the wave-frequency components exists in the surge response spectra. The peaks of the wave-frequency surge response spectra, the heave and pitch response spectra increase with the increase in H_s , but the corresponding frequencies do not change. The increase in the spectral peaks and the constant peaked frequencies can be inferred from Fig. 7a and Eq. (13).

Fig. 8a shows the wave spectra under case 1b. When H_s is constant, the area of the wave spectrum is constant. It is observed from Fig. 8a that as T_p increases, the spectral peak increases, the corresponding frequency decreases, and the spectral shape becomes narrower. It is found from Fig. 8b that as T_p increases, the peak of the surge low-frequency response spectrum decreases, and the corresponding frequency shifts to the left. The shape of the wave spectrum becomes narrower, resulting in a smaller integral value of the wave spectrum term $S(\omega)S(\omega + \Delta\omega)$ in Eq. (15). In addition, the QTFs of the low-frequency wave force depends on the platform itself, not T_p . Therefore, as T_p increases, the area of the second-order low-frequency wave force spectrum increases, as shown in Fig. 9. Then, according to Eq. (18), it can be inferred that as T_p increases, the surge low-frequency STD decreases. As for the wave-frequency component of the surge response spectrum, it is observed from Fig. 8b that as T_p increases, the peak increases, and the corresponding frequency shifts to the left. Fig. 10a shows the RAOs of surge at the wave-frequency range under case 1b. It can be seen from Fig. 10a that as T_p increases, the RAO increases. According to Eq. (14), it can be inferred that the surge wave-frequency STD increases with the increase in T_p . Regarding the heave motion, it is observed from Fig. 8c that at the frequency range of 0.25–0.5 rad/s, the characteristics of the response spectra and the wave-frequency components of the surge response spectra are similar. As T_p increases, the peak becomes

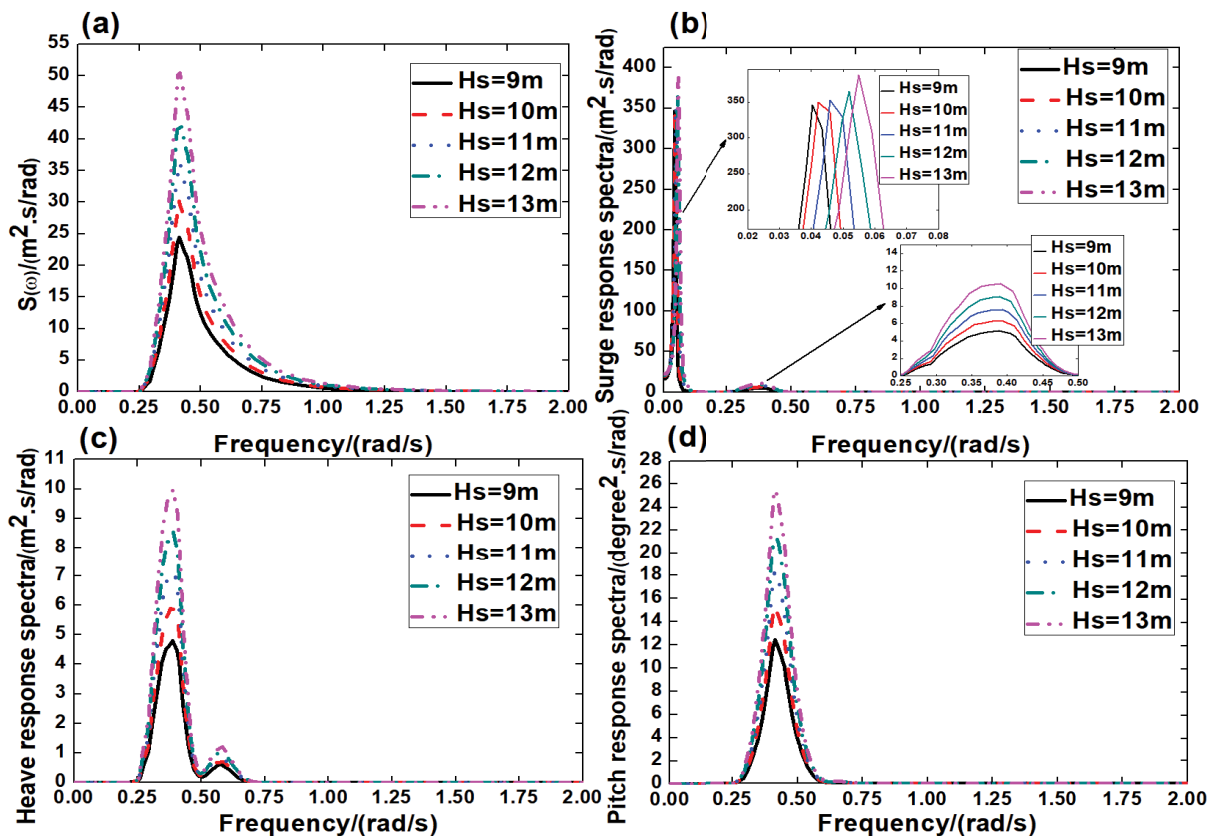


Fig. 7. Wave spectra and motion response spectra under case 1a.

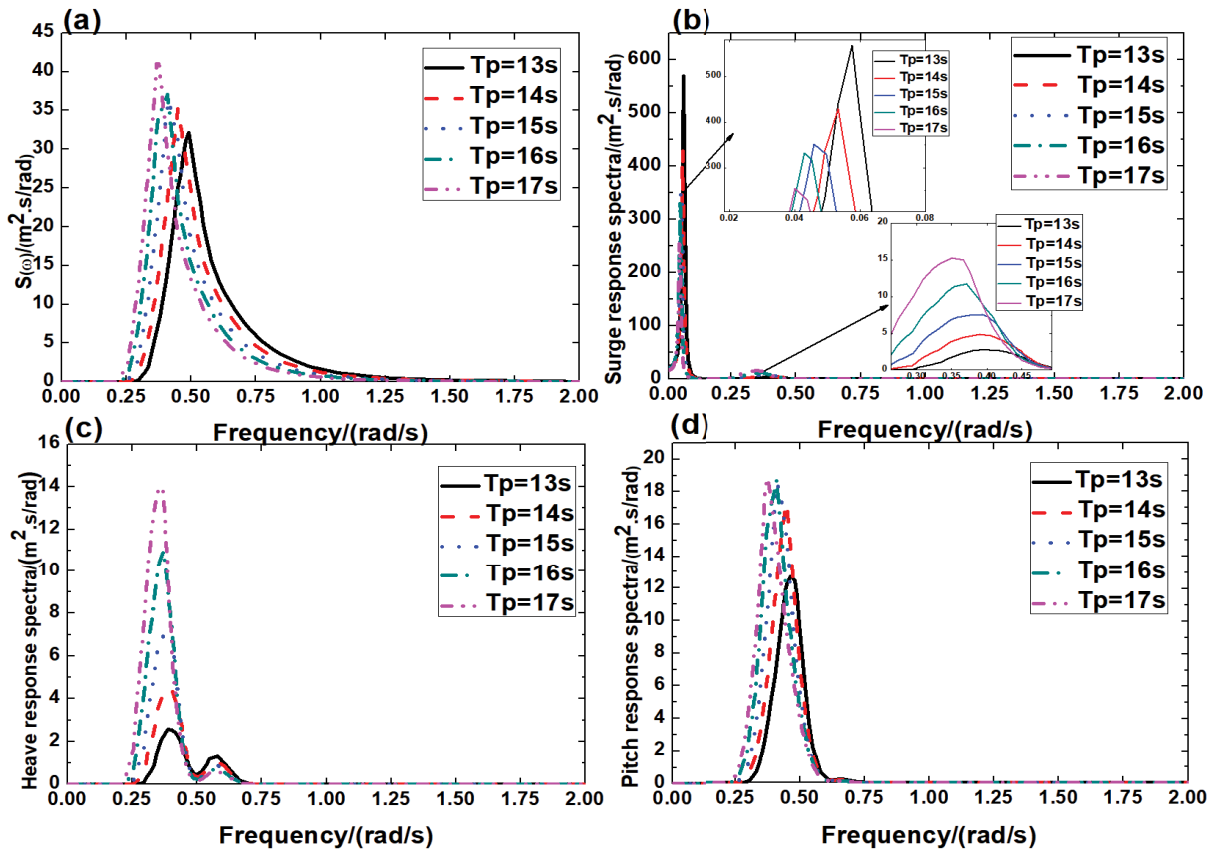


Fig. 8. Wave spectra and motion response spectra under cases 1b.

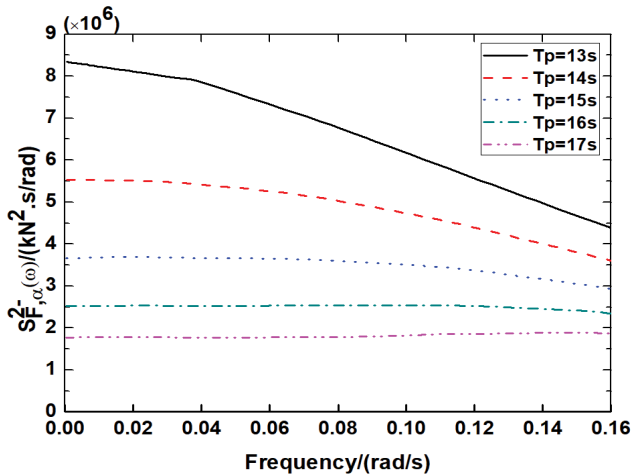


Fig. 9. The second-order low-frequency wave force spectrum under case 1b.

larger, and the corresponding frequency shifts to the left. However, at the frequency range from 0.5–0.7 rad/s, as T_p increases, the peak becomes smaller, and the corresponding frequency remains unchanged. Fig. 10b shows the RAOs of heave motion under different T_p . It can be found from Fig. 10b that at the frequency range from 0.25–0.5 rad/s, the heave RAO increases with the increase

in T_p . However, at the frequency range from 0.5–0.7 rad/s, the heave RAO slightly decreases as T_p increases. Then, the characteristics of the heave response spectra can be explained according to Eq. (13). It can be concluded that at the frequency range of 0.25–0.5 rad/s, both wave spectrum and RAO have an influence on Eq. (13). But at the frequency range of 0.5–0.75 rad/s, the contribution of RAO to Eq. (13) is more obvious. As for the pitch motion, it is observed from Fig. 8d that the characteristics of the response spectra are similar to the wave-frequency components of the surge response spectra. In addition, it can be found from Fig. 8d that as T_p increases, the variation in the response spectrum area gradually decreases. When $T_p = 16$ and 17 s, the areas of the response spectra are almost the same. These characteristics of the pitch response spectral areas can be reflected in Fig. 7b. Fig. 10c shows the RAOs of the pitch motion under case 1b. It can be seen from Fig. 10c that as T_p increases, the RAO increases. When $T_p = 16$ and 17 s, the RAOs of the pitch motion are almost the same. Then, according to Eq. (13), the characteristics of the pitch response spectra can be inferred.

7. Conclusions

This paper studies the effects of mooring line hydrodynamic coefficients and wave parameters on the FPSO motions. Based on a coupled time-domain analysis code,

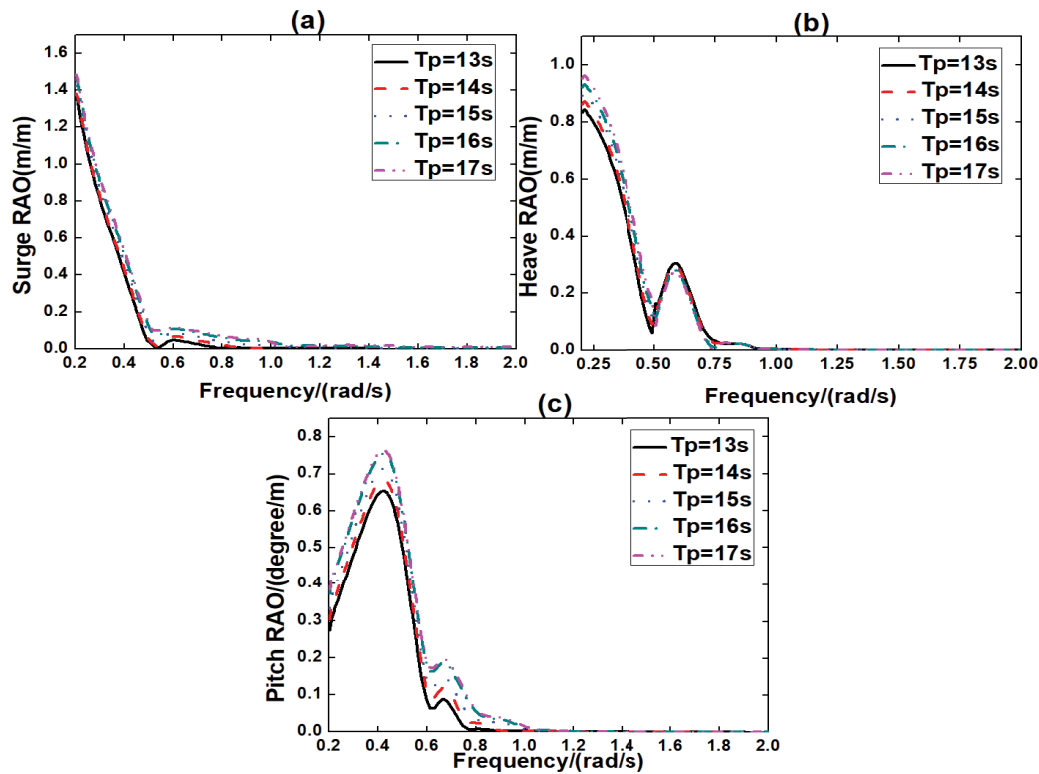


Fig. 10. RAOs of the floating production storage and offloading motions under case 1b.

some conclusions are obtained based on the STDs and response spectra of the time histories:

- As the mooring line hydrodynamic coefficients increase, the sensitivity of the low-frequency component of surge motion to wave parameters decreases. However, the sensitivity of wave-frequency motion with respect to wave parameters remains unchanged. This means that the increase in hydrodynamic coefficients is of great help to the suppression of low-frequency motion under variable sea conditions, thereby extending the fatigue life of mooring lines and risers.
- As H_s increases, the STD of the FPSO dynamic response increase. Especially for the low-frequency component of surge motion, the corresponding STD increases significantly. This will aggravate the fatigue damage of mooring lines and risers under the wave conditions with large H_s . In addition, the STD of low-frequency motion has a quadratic relationship with H_s , while the STD of wave-frequency motions have a linear relationship with H_s . The degree of freedom of motion of which the natural period is close to the spectral peak period varies obviously with respect to H_s . Therefore, when the platform is designed, it should be avoided that the natural period of wave-frequency motion is close to the main wave periods at the operating sea area. In addition, as H_s increases, the peak of the low-frequency response spectrum increases and shifts to the right. The peak of the wave-frequency response spectrum increases and the corresponding frequency remains constant.

- As H_s increases, the STD of low-frequency motion decreases, and the STDs of wave-frequency motion increase. With the increase in T_p , the variation trend of STDs of the pitch motion slows down. The wave-frequency STD of the surge motion and the STD of the heave motion have a roughly linear relationship with T_p . In addition, with the increase in T_p , the peak of the low-frequency response spectrum decreases but the peak of the wave-frequency response spectrum increases. Their corresponding frequencies all shifts to the left.

These conclusions are helpful to understand the effects of mooring line hydrodynamic coefficients and wave parameters on the FPSO dynamic behavior. They have a great reference value for the initial design of the FPSO system.

Acknowledgment

The authors would like to acknowledge the support of the National Natural Science Foundation of China (Grant No. 52001138), the National Natural Science Foundation of Jiangsu Province (Grant No. BK20201029; 20KJB416005) and the National Natural Science Foundation of China, 52101356.

References

- [1] J.E.W. Wichers, A Simulation Model for a Single Point Moored Tanker, Ph.D. Thesis, Delft University, The Netherlands, 1988.
- [2] T. Jiang; T.E. Schellin, Motion prediction of a single-point moored tanker subjected to current, wind and waves, J. Offshore Mech. Arct. Eng., 112 (1989) 83–90.

- [3] J.M. Heurtier, P. Le Buhan, E. Fontaine, C. Le Cunff, F. Biolley, C. Berhault, Coupled Dynamic Response of Moored FPSO With Risers, Proceedings of the Eleventh (2001) International Offshore and Polar Engineering Conference, Stavanger, Norway, 2001, pp. 319–326.
- [4] B.W. Kim, H.G. Sung, J.H. Kim, S.Y. Hong, Comparison of linear spring and nonlinear FEM methods in dynamic coupled analysis of floating structure and mooring system, *J. Fluid Struct.*, 42 (2013) 205–227.
- [5] L.M. Bergdahl, I. Rask, Dynamic vs. Quasi-Static Design of Catenary Mooring System, Proceedings of the 19th Offshore Technology Conference, Houston, Texas, USA, 1987, pp. 398–404.
- [6] X.H. Chen, J. Zhang, W. Ma, On dynamic coupling effects between a spar and its mooring lines, *Ocean Eng.*, 28 (2001) 863–887.
- [7] C.E. Dorado, J.C. Molano, Microthermometry and raman spectroscopy of fluid inclusions from El vapor gold mineralizations, Colombia, *Earth Sci. Res. J.*, 22 (2018) 151–158.
- [8] Y. Inoue, H. Miyabe, X. Weiyi, M. Nakamura, Comparative Study on the Quasi-Static Analyses and Dynamic Simulations for Estimating the Maximum Tensions of Mooring Lines, Proceedings of the 1st International Offshore and Polar Engineering Conference, Edinburgh, UK, 1991, pp. 236–242.
- [9] H. Ormberg, K. Larsen, Coupled analysis of floater motion and mooring dynamics for a turret-moored ship, *Appl. Ocean Res.*, 20 (1988) 55–67.
- [10] A. Tahar, Z. Ran, M.H. Kim, Hull/Mooring/Riser Coupled Spar Motion Analysis With Buoyancy-Can Effect, The Twelfth International Offshore and Polar Engineering Conference, Kitakyushu, Japan, 2002, pp. 223–230.
- [11] G.Q. Lyu, H.Q. Zhang, J.C. Li, Effects of incident wind/wave directions on dynamic response of a SPAR-type floating offshore wind turbine system, *Acta Mech. Sin.*, 35 (2019) 954–963.
- [12] O.A. Montasir, A.J. Idris, G.Z. Matthew, Effects of water depth, mooring line diameter and hydrodynamic coefficients on the behavior of deepwater FPSOs, *Ain Shams Eng. J.*, 11 (2020) 727–739.
- [13] J. Mohammed, E.I. Abdulrahman, A. Suhail, Z.J. Mohd, Effect of moorings drag and inertia on response of spar platform, *KSCE J. Civ. Eng.*, 21 (2017) 2503–2513.
- [14] M. Ezoji, A.R.M. Gharabaghi, H. Gol-Zaroudi, The Effects of Wave Parameters on Motion Performance of Semi-Submersible Platforms, G. Soares, Santos, Eds., Maritime Technology and Engineering, Taylor & Francis Group, London, 2014.
- [15] J.T. Lopez, L.B. Tao, Non-Linear Coupled Analysis for a Moored FPSO in Deepwater of the Gulf of Mexico, In the 33rd International Conference on Ocean, Offshore and Arctic Engineering, San Francisco, California, USA, 2014.
- [16] M.F. Mohd Hanapiah, S. Saad, Z. Ahmad, Hydrodynamic modelling in inshore reef area within Kuantan Coastal Region, *J. CleanWAS*, 4 (2020) 1–7.
- [17] B. Singh, P. Sihag, A. Parsaie, A. Angelaki, Comparative analysis of artificial intelligence techniques for the prediction of infiltration process, *Geol. Ecol. Landscapes*, 5 (2021) 109–118.
- [18] N. Rini, V.J. Kurian, M.S. Liew, A. Whyte, Coupled Analysis for the Effect of Wave Height on FPSO Motions, In the 3rd International Conference on Civil, Offshore and Environmental Engineering, ICCOEE, Malaysia, 2016, pp. 69–74.
- [19] J. Wu, Q. Meng, X. Fu, Y. Ma, M. Sun, N. Sun, W. Tan, Study on the relationship between multi-stage strike-slip mechanism and basin evolution in Fangzheng Fault Depression, *Earth Sci. Res. J.*, 22 (2018) 335–339.
- [20] J.F. Du, S.Q. Wang, A.T. Chang, H.J. Li, An investigation on low frequency fatigue damage of mooring lines applied in a semi-submersible platform, *J. Ocean Univ. China*, 15 (2016) 438–446.
- [21] Z.X. Zhao, W.H. Wang, W. Shi, X. Li, Effects of second-order hydrodynamics on an ultra-large semi-submersible floating offshore wind turbine, *Structures*, 28 (2020) 2260–2275.
- [22] C. Barrera, I.J. Losada, R. Guanache, L. Johanning, The influence of wave parameter definition over floating wind platform mooring systems under severe sea states, *Ocean Eng.*, 172 (2019) 105–126.
- [23] J.N. Newman, Second-Order, Slowly-Varying Forces on Vessels in Irregular Waves, International Symposium on the Dynamics of Marine Vehicles and Structures in Waves, London, 1974, pp. 182–186.
- [24] M. Hall, A. Goupee, Validation of a lumped-mass mooring line model with DeepCwind semisubmersible model test data, *Ocean Eng.*, 104 (2015) 590–603.
- [25] J.A. Pinkster, Low-frequency phenomena associated with vessels moored at sea, *Soc. Pet. Eng. J.*, 15 (1975) 487–494.
- [26] V.L.F. Matos, A.N. Simos, S.H. Sphaier, Second-order resonant heave, roll and pitch motions of a deep-draft semi-submersible: theoretical and experimental results, *Ocean Eng.*, 38 (2011) 2227–2243.